Theor Chem Acc (2017) 136:93
DOI 10.1007/s00214-017-2126-7

REGULAR ARTICLE

Promethium-doped silicon clusters $PmSi_n$ (n = 3–10) and their anions: structures, thermochemistry, electron affinities and magnetic moments

Shuang He[1,2] · **Jucai Yang**[1,3]

Received: 10 May 2017 / Accepted: 31 July 2017 / Published online: 4 August 2017

Abstract The equilibrium geometries, electronic structures and electronic properties of $PmSi_n$ (n = 3–10) clusters were systematically investigated using the ABCluster global search technique combined with density functional methods. The results revealed that the most stable structure of neutral $PmSi_n$ and their anions can be viewed as replacing a Si atom of the ground state structure of Si_{n+1} with a Pm atom. The adiabatic electron affinities of $PmSi_n$ are evaluated, and they differ little from those of $SmSi_n$ and $EuSi_n$. Analyses of HOMO–LUMO gaps showed that introducing Pm atom to Si cluster can significantly improve photochemical reactivity of the cluster. And the improved effects are as good as those of the introducing Sm and Eu atom to Si cluster. The NPA calculations indicated that the 4*f* electrons of Pm atom in $PmSi_n$ (n = 3–10) clusters hardly participate in bonding and provide the total magnetic moments. Dissociation energy (DE) of rare earth metal (REM) atom from the lowest energy structure of $REMSi_n$ (n = 3–10) and their anions was calculated. The DEs of $PmSi_n$, $SmSi_n$ and $EuSi_n$ are nearly identical. The DEs of $PmSi_n^-$, $SmSi_n^-$ and $EuSi_n^-$ are also nearly equal, and they are smaller than those of $HoSi_n^-$ and $PrSi_n^-$.

✉ Jucai Yang
yangjc@imut.edu.cn

[1] School of Chemical Engineering, Inner Mongolia University of Technology and Inner Mongolia Key Laboratory of Theoretical and Computational Chemistry Simulation, Hohhot 010051, People's Republic of China

[2] Inner Mongolia Vocational College of Chemical Engineering, Hohhot 010070, People's Republic of China

[3] School of Energy and Power Engineering, Inner Mongolia University of Technology, Hohhot 010051, People's Republic of China

Keywords $PmSi_n$ · The ground state structure · Electron affinity · Dissociation energy · Electronic property

1 Introduction

Over the past few decades, silicon-based clusters have attracted a great deal of attentions due to their acknowledged importance not only in the modern microelectronics industry, but also as building blocks for the developing new and tunable silicon-based nanomaterials [1–8]. Different from carbon clusters which usually show sp^2 hybridization, pure silicon clusters favor the sp^3 hybridization because Si atom has a larger *p*-orbital than C atom, and C atom has larger *s*-orbital than Si atom [9]. As a result, the pure Si clusters are chemically reactive because of the presence of unsaturated dangling bonds and are unsuitable as nanoscale building blocks [10, 11]. It has been found that doping an appropriate foreign atom such as transitional metal (TM) atom and rare earth metal (REM) atom inside silicon clusters can not only solve the deficiency, but also influence impressively the fascinating physical and chemical properties such as narrow HOMO–LUMO gaps, high magnetic moments, bright photoluminescence of these silicon-based clusters [12–18].

Up to date, there have been some scientific researches on REM-doped silicon clusters. For instance, Nakajima and co-workers firstly studied doping REM atoms into silicon cluster anions $REMSi_n^-$ (REM = Tb, Ho, Lu, n = 6–20) clusters by using photoelectron spectra (PES) and reported their electronic structures and threshold energies of electron detachment [1, 2]. Subsequently, Grubisic et al. [3, 4] reported the PES of $REMSi_n^-$ (REM = Ho, Gd, Pr, Sm, Eu, Yb; n = 3–13) and found that the PES can be categorized as three types in light of their motifs. Motivated by these experimental observations, some theoretical simulation

and computation have been carried out for $REMSi_n$ clusters including $PrSi_n$ [7, 19], $SmSi_n$ [20], $EuSi_n$ [21, 22], $GdSi_n$ [23], $HoSi_n$ [11, 16, 24], $YbSi_n$ [25–27] and $LuSi_n$ [28] to evaluate their equilibrium configuration and electronic properties such as relative stability, HOMO–LUMO gap, adiabatic electron affinity (AEA), magnetic moment and so forth. Recently, we [29–35] investigated the most stable structures and properties of $PrSi_n$, $SmSi_n$, $EuSi_n$, $GdSi_n$, $HoSi_n$, $YbSi_n$ and $LuSi_n$ ($n \leq 10$) and their anions and concluded that (1) The $REMSi_n$ can be divided into two types according to the situation of 4*f* electron participation in bonding. One (corresponding to "A" type in Ref. [4]) is that the 4*f* electron hardly participates in bonding, and another (corresponding to "B" in Ref. [4]) is that the 4*f* electron prefers to participate in bonding. (2) The double-hybrid mPW2PLYP and/or B2PLYP functional can accurately predict electron affinities of $REMSi_n$ including both types of A and B. The pure and single-hybrid density functional theory such as popular PBE, PBE0, TPSSh and B3LYP, especially TPSSh, can only accurately evaluate the electron affinities for $REMSi_n$ of type A. Therefore, we applied the mPW2PLYP [36] methods in this paper to the determination of equilibrium configurations and electronic properties (including relative stability, HOMO–LUMO gap, AEA, magnetic moment and charge transfer characteristics) of neutral $PmSi_n$ ($n = 3$–10) and their anions with the target of understanding which type (A, B, or AB) $PmSi_n$ clusters belong to and how their properties differ from those of bare Si clusters and other $REMSi_n$ species. Our calculations will provide not only specific guidance for the study of medium-size clusters but also strong motivation for further experimental studies of these important $PmSi_n$ clusters and their anions.

2 Computational schemes

It is well known that locating the global minimum of the large clusters is usually a rather difficult task. The possibility of missing the ground state structure exists. For small size clusters, this problem can be solved by using a global optimization technique. But with the cluster size increasing, the number of local minimal isomers increases exponentially. The complex distribution of these huge numbers of local minimal isomer makes the potential energy surface locally very rugged, making an "ergodic" sampling on the potential energy surface of the large clusters (especially for heteroatom clusters) by computer simulation nearly impossible [37]. On the other hand, the most stable structure of $SmSi_n$, $EuSi_n$ and $YbSi_n$ is substitutional structure [30, 31, 34]. Therefore, apart from the ABCluster [37], the "substitutional structure" is also taken into account in order to ensure the lowest energy structure can be selected into initial configuration as much as possible. The detailed description for the ABCluster global search technique combining with the Gaussian 09 codes [38] is as follows. The ABCluster uses the "artificial bee colony" (ABC) algorithm to perform the global optimization. Of course, it can be used as random generator only. The first step is that for $n \leq 7$, 100 initial geometries of $PmSi_n$ generated by the ABCluster are selected (the ABCluster codes are black-box program, and the first geometry is generated randomly), and 300 are selected for $n \geq 8$. Then, the TPSSh functional [39] combining with SMALL basis sets (which contains 6-31G basis set for Si atoms and ECP50MWB basis set [40] for Pm atom) is chosen to optimize the initial geometries of each cluster one by one with doublet electronic state. The second step is that the isomers with their energy differences within 0.8 eV from the lowest energy isomer from the first step for each species are chosen and reoptimized by using the TPSSh functional combined with the LARGE basis sets (which contains Stuttgart-ECP basis set [41, 42] for Pm and the cc-pVTZ [43] for Si atoms). In the third step, the isomers from the second step with their energy value within 0.8 eV from the lowest energy isomer are optimized by using the mPW2PLYP/LARGE method. The substitutional structures for $PmSi_n$ are generated by replacing each Si of the ground state structure of Si_{n+1} with a Pm atom. In fact, our experience is that for pure Si_n cluster with $n \leq 11$, the ground state structures predicted by using the ABCluster method with 100 initial geometries are the same as the known ones reported previously. For $REMSi_n$ clusters, when $n \leq 7$, the 100 initial geometries generated from the ABCluster method include all of the substitutional structures. However, from $n = 8$, even 500 initial geometries generated from the ABCluster method do not include all of the substitutional structures. For instance, the most stable geometries of $PmSi_8$ (and/or $PmSi_8^-$) and $PmSi_9^-$ belong to substitutional structure, but cannot be found by ABCluster method. It is to say that the selection of the initial geometries to consider two types is necessary. In addition, only sextuplet electronic state was considered for neutral $PmSi_n$ clusters. The reason is that if 4*f* electrons of Pm atom participate scarcely in bonding (it is to say that electron configurations of Pm is $[core]6s^24f^55d^0$), the spin multiplicities of neutral $PmSi_n$ are sextuplet. If 4*f* electrons are involved in bonding (the electron configurations of Pm is $[core]6s^24f^45d^1$), the spin multiplicities of neutral $PmSi_n$ are still sextuplet. (Take $PmSi_{10}$ as an example for this point of view, we have examined the energies of $PmSi_{10}$ isomers with quartet and octuplet electronic states. The results revealed that the energies of octuplet electronic states are higher than that of sextuplet electronic state. For quartet electronic state, there are serious spin contamination). For their anions, the quintuplet and septet electronic states were considered for $n = 3$–6. The results revealed that the ground state of $PmSi_n^-$ anions is septet electronic state. That is, the 4*f* electrons hardly participate in bonding.

Although many structures were gotten, only several selected isomers were reported.

Harmonic frequency analysis was performed only at the TPSSh/LARGE level of theory to assure that the geometries presented in this work are local minima. The mPW2PLYP geometries were applied in single-point calculations with diffuse functions (which contains the aug-cc-pVTZ basis sets [43] for Si atoms and Stuttgart RSC 1997 ECP basis set augmented with 2*pdfg* diffuse functions [44] for Pm atom, denoted as aug-LARGE). Finally, the mPW2PLYP energies at 0 K are obtained by adding the ZPVE (zero point vibration energy) of the TPSSh. The energies of mPW2PLYP/aug-LARGE//mPW2PLYP/LARGE were used for calculations of properties such as AEA and dissociation energies. All of the calculations were performed using the GAUSSIAN 09 soft package [38]. It is reasonable to adopt the double-hybrid mPW2PLYP scheme. The average absolute deviation of the mPW2PLYP from experiment for 35 calculated AEA of $REMSi_n$ (excluded $PrSi_6$) including type of A and B is only 0.05 eV as shown in Table 1. In our previous study, ECP-28MWB small-core relativistic potentials and segmented (SEG) valence Gaussian valence basis sets (namely "SEG/ECP") [45] were employed for the REM atoms [29–33]. At present, they are replaced by the Stuttgart-ECP basis sets. The reason is that (1) SEG/ECP basis set is sometimes excessive mixing of frozen core and valence orbitals; (2) it can save computation time; and (3) the result is agreement with experimental data as described above. The double-hybrid mPW2PYP is susceptible to the initial geometry. A poor initial geometry can result in convergence failure for mPW2PLYP scheme. On the other hand, the cost for frequency calculation of mPW2PLYP is expensive. So the TPSSh method is used for optimization of initial geometries. Our experience is that apart from the TPSSh, the PBE, PBE0 and B3LYP methods can also be recommended for optimization of initial geometries.

Table 1 Deviations of calculated adiabatic electron affinity (AEA) from experiment

Species	AEA		
	mPW2PLYP	Expt.[b]	Deviation
$SmSi_3$	1.45	1.40 ± 0.05	0.05
$SmSi_4$	1.59	1.50 ± 0.05	0.09
$SmSi_5$	1.65	1.60 ± 0.05	0.05
$SmSi_6$	1.53	1.5 ± 0.1	0.03
$SmSi_7$	1.65	1.6 ± 0.1	0.05
$SmSi_8$	1.77	1.7 ± 0.1	0.07
$SmSi_9$	1.99	2.10 ± 0.10	−0.11
$SmSi_{10}$	1.94	2.00 ± 0.10	−0.06
$EuSi_3$	1.47	1.45 ± 0.05	0.02
$EuSi_4$	1.66	1.6 ± 0.05	0.06
$EuSi_5$	1.70	1.70 ± 0.05	0.00
$EuSi_6$	1.60	1.55 ± 0.05	0.05
$EuSi_7$	1.71	1.70 ± 0.05	0.01
$EuSi_8$	1.79	1.75 ± 0.05	0.04
$EuSi_9$	2.13	2.20 ± 0.1	−0.07
$EuSi_{10}$	1.99	2.00 ± 0.1	−0.01
$GdSi_2$	1.30	1.30 ± 0.05	0.00
$GdSi_3$	1.47	1.60 ± 0.05	−0.13
$GdSi_4$	2.12	2.15 ± 0.05	−0.03
$GdSi_5$	1.89	1.95 ± 0.05	−0.06
$GdSi_6$	2.10	2.0 ± 0.5	0.10
$GdSi_7$	2.31	2.3 ± 0.1	0.01
$GdSi_8$	2.51	2.5 ± 0.2	0.01
$GdSi_9$	2.96	2.9 ± 0.1	0.06
$HoSi_4$	2.20	2.20 ± 0.1	0.00
$HoSi_5$	2.01	2.05 ± 0.05	−0.04
$HoSi_6$	2.36	2.4 ± 0.0043	−0.04
$HoSi_7$	2.33	2.4 ± 0.1	−0.07
$HoSi_8$	2.57	2.7 ± 0.2	−0.13
$HoSi_9$	2.92	2.9 ± 0.1	0.02
$PrSi_4$	2.10	2.0 ± 0.1	0.10
$PrSi_5$	1.87	1.9 ± 0.1	−0.03
$PrSi_6$	1.61	2.1 ± 0.1	−0.49
$PrSi_7$	2.39	2.4 ± 0.1	−0.01
$PrSi_8$	2.53	2.5 ± 0.2	0.03
$PrSi_9$	2.85	2.8 ± 0.1	0.05

AEAs and deviations in eV. Deviation = Theory − Experiment. The theoretical AEAs are calculated by the mPW2PLYP/aug-LARGE//mPW2PLYP/LARGE method without ZPVE. The ground state structures for $SmSi_n$, $EuSi_n$, $GdSi_n$, $HoSi_n$ and $PrSi_n$ and their anions see Refs. [29–33]

[a]See Refs. [2–4] for experimental references excluded $GdSi_4$, $PrSi_4$ and $HoSi_4$, of which experimental values see Refs. [29, 32, 33]

3 Results and discussion

3.1 Neutral and anionic geometries

The optimized geometries of neutral $PmSi_n$ (n = 3–9) at the mPW2PLYP/LARGE level are shown in Fig. 1. For $PmSi_3$, two isomers are reported. One is a *planar rhombus* (**3a**) with $^6B_2$ ground state. And another is a *tetrahedron* (**3b**) with $^6A_1$ electronic state. Energetically, it is less stable than that of **3a** by 0.74 eV. For $PmSi_4$, three isomers are presented. The **4a** structure of $^6A''$ is predicted to be the ground state. Both **4a** and **4c** can be regarded as being derived from the ground state *trigonal bipyramid* structure of Si_5 [46, 47] by replacing a Si atom at different positions with a Pm atom. The geometry **4b** can be regarded as attaching a Pm atom to the ground state *planar rhombus* structure of Si_4 [46, 47]. For $PmSi_5$, two isomers are reported. Both **5a** and **5b** belong to substitutional structure. The **5a** structure of $^6A''$ electronic state is predicted to be the ground state structure,

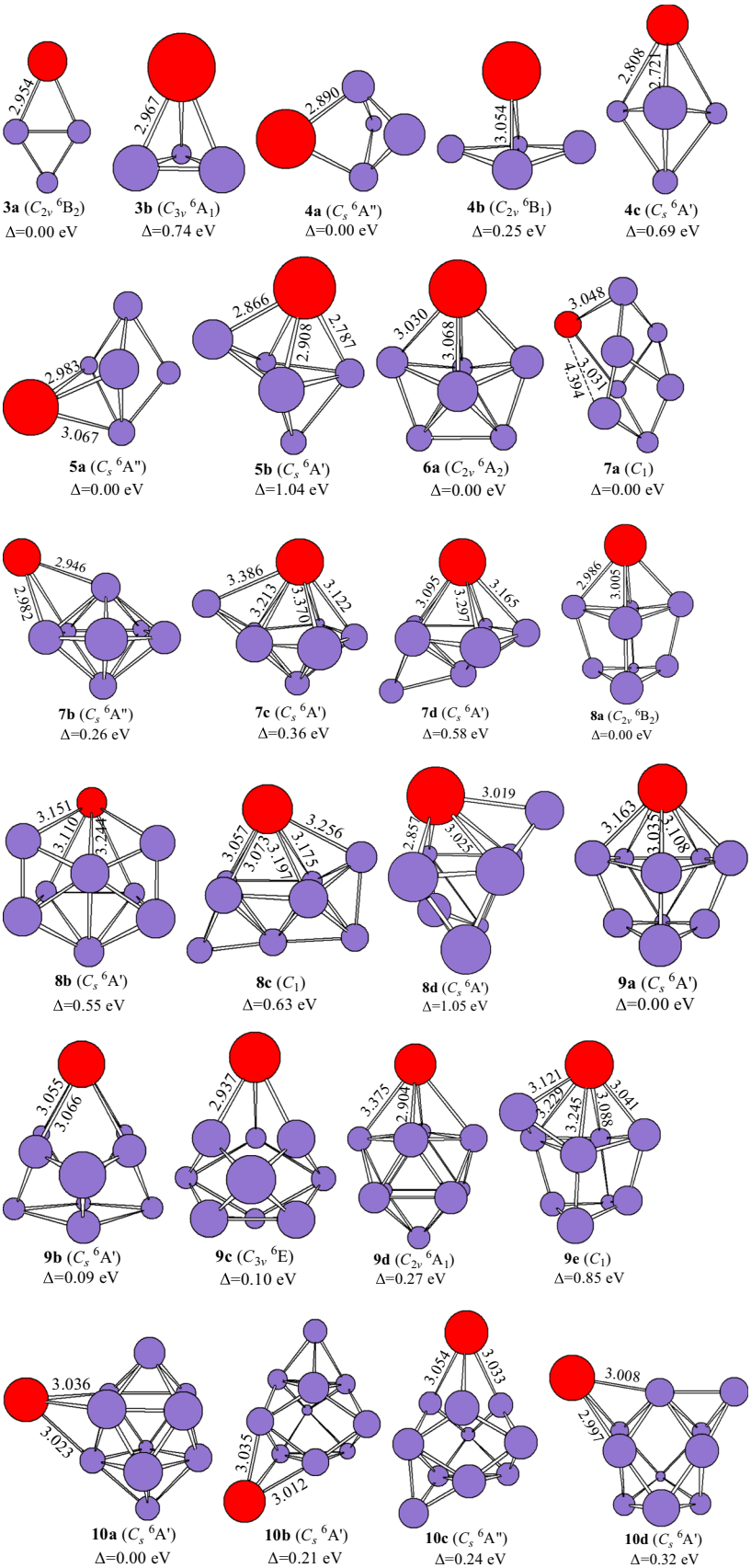

Fig. 1 Neutral geometries optimized with the mPW-2PLYP scheme. The Pm–Si bond lengths are in angstroms. The relative energies, Δ, are obtained at the mPW2PLYP/LARGE level and in eV

analogous to the ground state structure of $SmSi_5$ and $EuSi_5$ [30, 31]. The **5b** isomer of $^6A'$ electronic state is similar to the ground state structure of $PrSi_5$, $GdSi_5$ and $HoSi_5$ [29, 32, 33]. For $PmSi_6$, the **6a** structure of $^6B_1$ ground state is a *pentagonal bipyramid* with Pm atom positioning horizontal axis, analogous to the ground state structure of $REMSi_6$ (REM = Pr, Sm, Eu, Gd, Ho, Yb, Lu) [29–35]. For $PmSi_7$, four isomers are reported. The structure **7a**, which can be viewed as replacing a Si of ground state structure of Si_8 [47, 48] with a Pm atom, is predicted to be the ground state structure, analogous to the ground state structure of $SmSi_7$ and $EuSi_7$ [30, 31]. The **7b** isomer of $^6A''$ electronic state can be regarded as attaching a Pm atom to the ground state *pentagonal bipyramid* structure of Si_7 [46, 47]. Both **7c** and **7d** isomers possess $^6A'$ electronic state. The **7d** geometry is similar to the ground state structures of $GdSi_7$ and $HoSi_7$ [32, 33]. For $PmSi_8$, four isomers are presented. The isomer **8a** belongs to substitutional structure and is the most stable structure with $^6B_2$ ground state. The second lowest structure **8b** is similar to beetle with $^6A'$ electronic state. The isomers **8b**, **8c** and **8d** are significantly higher in energy than that of **8a** substitutional structure. For $PmSi_9$, five isomers are presented. The **9a**, **9b** and **9c** geometries can be regarded as replacing a Si atom at different position of ground state structure of Si_{10} [47, 48] with a Pm atom. They compete with each other for the ground state structure of $PmSi_9$ because their energy differences differ little from each other. The **9a** structure, analogous to the ground state structure of $SmSi_9$ and $EuSi_9$ [30, 31], is only more stable in energy than the **9b** and **9c** isomers by 0.09 and 0.10 eV, respectively. The **9d** isomer, *bicapped tetragonal antiprism*, is similar to the ground state structure of $PrSi_9$ [29]. The **9e** isomer can be viewed as attaching a Si atom to the ground state structure of $PmSi_8$. Both **9d** and **9e** structures are less stable in energy than that of **9a**. For $PmSi_{10}$, four isomers are reported. The **10a** structure, analogous to the ground state structure of $SmSi_{10}$ and $EuSi_{10}$ [30, 31], can be regarded as replacing a Si atom of *tricapped tetragonal antiprism* of Si_{11} [48] with a Pm atom. It is predicted to be the most stable structure with $^6A'$ ground state. The **10b** isomer can be viewed as attaching a Pm atom to the ground state *tetracapped trigonal prism* of Si_{10} [48]. Energetically, the **10b**, **10c** and **10d** isomers are less stable than that of **10a** by 0.21, 0.24 and 0.32 eV, respectively. Take $PmSi_{10}$ as an example, their energies of quartet and octuplet electronic states are examined. The results revealed that the energies of **10a**–**10d** isomers with octuplet electronic states are higher than those with sextuplet electronic state by 0.95, 0.80, 0.99 and 0.87 eV, respectively. For quartet electronic state, there are serious spin contamination (expectation values of S^2 are about 4.64–5.75).

The optimized geometries of anion $PmSi_n^-$ (n = 3–9) at the mPW2PLYP level are exhibited in Fig. 2. The Spin, S^2 operator values and relative energy of anion $PmSi_n^-$ (and neutral $PmSi_n$) are listed in Table 2. From Table 2, we can see that the energies of quintuplet electronic state for isomers **3a**$^-$, **5a**$^-$ and **6a**$^-$ are only 0.09, 0.09 and 0.04 eV above those of septet electronic states, respectively. Their S^2 operator analysis reveals that the results of quintuplet electronic state are not trustworthy because of spin contamination. The expectation values (7.01) of S^2 can be expanded for pure states with higher multiplicities. And hence, the septet ground state evaluated for the anions is trustworthy. For **3b**$^-$, **4a**$^-$ and **4b**$^-$ isomers of quintuplet electronic state, the spin contamination also occurs. Although the spin contamination does not occur for **4c**$^-$ and **6b**$^-$ isomers of quintuplet electronic state, of which energies are obviously higher.

For negatively charged ion $PmSi_n^-$ with n = 3–10, their ground state structures are predicted to be **3a**$^-$, **4a**$^-$, **5a**$^-$, **6a**$^-$, **7a**$^-$, **8a**$^-$, **9c**$^-$ and **10a**$^-$, respectively. This result is similar to that of negatively charged ion $SmSi_n^-$ and $EuSi_n^-$ [30, 31]. The **6b**$^-$ geometry, analogous to ground state structure of $PrSi_6$, $GdSi_6$ and $HoSi_6$, is higher in energy than that of **6a**$^-$ by 0.85 eV. The **7b**$^-$ isomer competes ground state with **7a**$^-$ structure because their energy difference falls in 0.10 eV.

Similar to the ground state structures of $REMSi_n$ (REM = Sm, Eu) and their anions [30, 31], the ground state structures of $PmSi_n$ (n = 3–10) and their anions can be regarded as replacing a Si atom of the most stable structures of Si_{n+1} clusters with a Pm atom. The most stable geometries of anionic clusters excluded $PmSi_9^-$ is similar to their corresponding to neutral ones. The Pm–Si bond distances of the anions are averagely longer than their corresponding neutral ones by 0.146 Å (obtained by using 28 bond distances of **3a**, **4a**, **5a**, **6a**, **7a**, **8a**, **9a**, **9c** and **10a** geometries).

3.2 Stability properties of clusters

It is well known that the dissociation energies (DEs) can be used to examine the relative stability of species. Here, the DEs are defined as the energy required for REM to dissociate from $REMSi_n$ or $REMSi_n^-$. The DEs calculated at the mPW2PLYP/aug-LARGE//mPW2PLYP/LARGE level for $PmSi_n$ and their anions are shown in Figs. 3 and 4, respectively. The DEs of $PrSi_n$, $SmSi_n$, $EuSi_n$, $GdSi_n$, $HoSi_n$ and their anions (of which ground state structures are taken from Refs. [29–33]) are also calculated at the same levels and plotted in Figs. 3 and 4, respectively, in order to facilitate comparison. From Figs. 3 and 4, we can see that (1) the DEs of $PmSi_n$ are close to those of $SmSi_n$, $EuSi_n$ and $HoSi_n$. The DEs of $GdSi_n$ are the largest among these data. The reason is that an unpaired d-orbital of Gd atom tends to form ionic polarization. As a result, the covalent bond character of the $GdSi_n$ system is enhanced [32]; (2) the consistent change trends of the DE vs n curves occur on all of these species. The larger the DEs, the more stable the

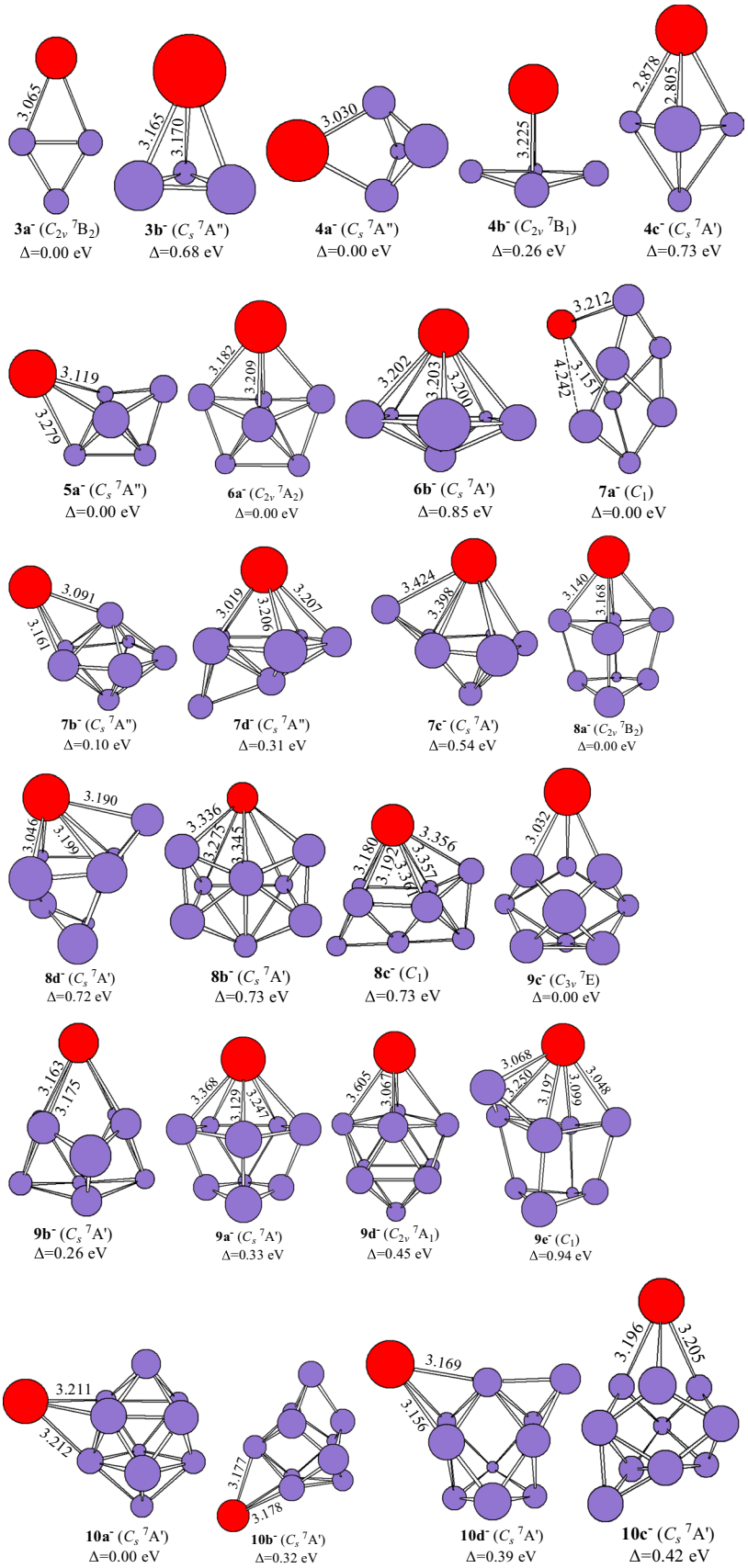

Fig. 2 Anion geometries optimized with the mPW-2PLYP scheme. The Pm–Si bond lengths are in angstroms. The relative energies, Δ, are obtained at the mPW2PLYP/LARGE level and in eV

Table 2 Spin (S), S^2 operator and relative energy (Δ) values of neutral $PmSi_n$ ($n = 3$–10) and their anions calculated with the mPW2PLYP scheme

Structure	S	S^2	Δ	Structure	S	S^2	Δ
3a	5/2	8.76	0.00	**4a**$^-$	6/2	12.00	0.00
3b	5/2	8.76	0.74		4/2	7.02	0.16
4a	5/2	8.77	0.00	**4b**$^-$	6/2	12.01	0.26
4b	5/2	8.76	0.25		4/2	7.01	0.34
4c	5/2	8.80	0.69	**4c**$^-$	6/2	12.04	0.73
5a	5/2	8.76	0.00		4/2	6.02	0.20
5b	5/2	8.80	1.04	**5a**$^-$	6/2	12.01	0.00
6a	5/2	8.76	0.00		4/2	7.01	0.09
7a	5/2	8.76	0.00	**6a**$^-$	6/2	12.00	0.00
7b	5/2	8.76	0.26		4/2	7.01	0.04
7c	5/2	8.76	0.36	**6b**$^-$	6/2	12.01	0.85
7d	5/2	8.76	0.58		4/2	6.02	0.50
8a	5/2	8.76	0.00	**7a**$^-$	6/2	12.02	0.00
8b	5/2	8.76	0.55	**7b**$^-$	6/2	12.01	0.10
8c	5/2	8.76	0.63	**7c**$^-$	6/2	12.02	0.54
8d	5/2	8.78	1.05	**7d**$^-$	6/2	12.05	0.31
9a	5/2	8.76	0.00	**8a**$^-$	6/2	12.01	0.00
9b	5/2	8.76	0.09	**8b**$^-$	6/2	12.01	0.73
9c	5/2	8.76	0.10	**8c**$^-$	6/2	12.01	0.73
9d	5/2	8.76	0.27	**8d**$^-$	6/2	12.03	0.72
9e	5/2	8.76	0.85	**9a**$^-$	6/2	12.01	0.33
10a	5/2	8.76	0.00	**9b**$^-$	6/2	12.01	0.26
10b	5/2	8.76	0.21	**9c**$^-$	6/2	12.02	0.00
10c	5/2	8.76	0.24	**9d**$^-$	6/2	12.01	0.45
10d	5/2	8.76	0.32	**9e**$^-$	6/2	12.04	0.94
3a$^-$	6/2	12.01	0.00	**10a**$^-$	6/2	12.01	0.00
	4/2	7.01	0.09	**10b**$^-$	6/2	12.01	0.32
3b$^-$	6/2	12.01	0.68	**10c**$^-$	6/2	12.01	0.42
	4/2	7.00	1.56	**10d**$^-$	6/2	12.01	0.39

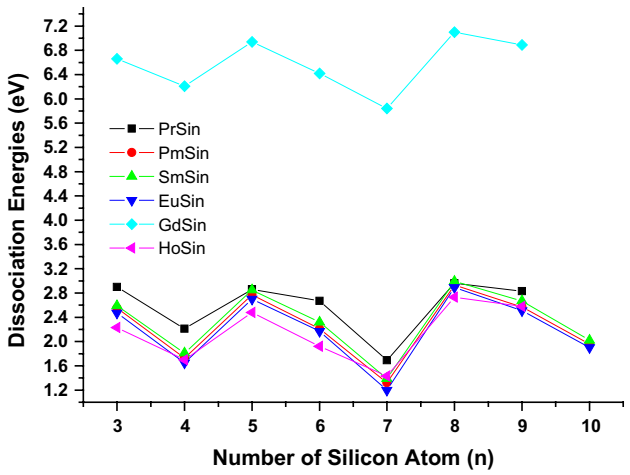

Fig. 3 Dissociation energy (DE, in eV) of neutral $REMSi_n$ (REM = Pm, Sm, Eu, Gd, Ho, Pr, $n \leq 10$) calculated at the mPW-2PLYP/aug-LARGE//mPW2PLYP/LARGE level of theory

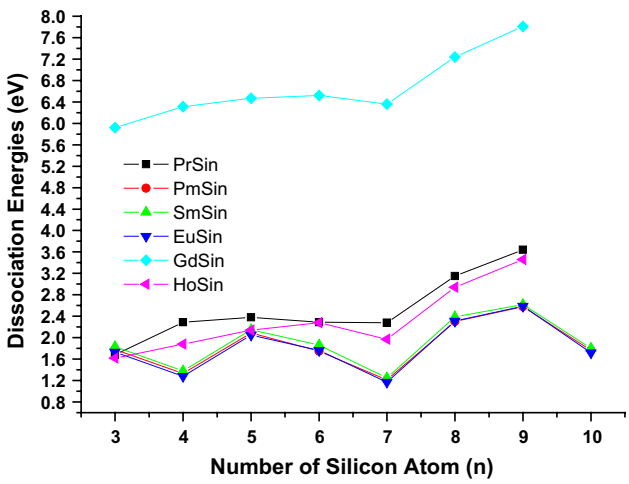

Fig. 4 Dissociation energy (DE, in eV) of anionic $REMSi_n$ (REM = Pm, Sm, Eu, Gd, Ho, Pr, $n \leq 10$) calculated at the mPW-2PLYP/aug-LARGE//mPW2PLYP/LARGE level of theory

clusters. So the $REMSi_4$ and $REMSi_7$ are less stable, and the $REMSi_5$ and $REMSi_8$ are more stable. (3) The DEs of $PmSi_n^-$, $SmSi_n^-$ and $EuSi_n^-$ are nearly identical. And they are smaller than those of $HoSi_n^-$ and $PrSi_n^-$. The reason can be explained as follows. The $PmSi_n$, $SmSi_n$ and $EuSi_n$ clusters belong to "A" type, while $HoSi_n$ and $PrSi_n$ species are "B" type. That is, an 4*f* electron of Ho and Pr atom transfers to 5d orbital and participates in bonding. This bond is equivalent to the SOMO (singly occupied molecular orbital). When these neutral clusters getting an electron become negatively charged ion, this additional electron going into the SOMO of neutral $REMSi_n$ (REM = Ho and Pr) becomes doubly occupied in the anion, which primarily localized on Si_n skeleton. However, the electron back donation from the Si_n skeleton to REM is induced and makes the bond between Si_n and REM strong. This property may be used for the separation of rare earth elements.

3.3 Electronic properties of clusters

AEA is not only electronic property but also a key spectroscopic value and vitally important for use in the chemical cycle. The AEA is defined as the energy difference between the neutral ground state structure and the anionic ground state structure. The AEA calculated at the mPW2PLYP level is listed in Table 3. There are no experimental values for comparison. Compared with $SmSi_n$ and $EuSi_n$, the AEAs of $PmSi_n$ differ little from those of $SmSi_n$ and $EuSi_n$. If the numerical size must be distinguished, the AEA of $PmSi_n$ is slightly larger than that of $SmSi_n$, but slightly smaller than that of $EuSi_n$ as shown in Fig. 5. We hope that our prediction will provide strong motivation for experimental studies of these important Pm-doped Si clusters and their anions.

HOMO–LUMO gap as an important physical property can also reflect the electronic property. The size dependence of the HOMO–LUMO gaps for the most stable structures of $PmSi_n$ (n = 3–10) calculated by the mPW2PLYP method is shown in Fig. 6. To facilitate comparison, the HOMO–LUMO gaps of $SmSi_n$, $EuSi_n$ and Si_n are also calculated and shown in Fig. 6. From Fig. 6, we can see that the consistent change trends of the HOMO–LUMO gap vs n curves exist in $PmSi_n$, $SmSi_n$ and $EuSi_n$, and the

Table 3 Adiabatic electron affinity (AEA) with ZPVE correction for PmSin (n = 3–10) species

Species	AEA	Species	AEA
$PmSi_3$	1.44 (1.45)	$PmSi_7$	1.68 (1.69)
$PmSi_4$	1.62 (1.63)	$PmSi_8$	1.74 (1.75)
$PmSi_5$	1.68 (1.69)	$PmSi_9$	2.05 (2.06)
$PmSi_6$	1.55 (1.55)	$PmSi_{10}$	1.95 (1.96)

Presented in eV. The values in parentheses are without ZPVE

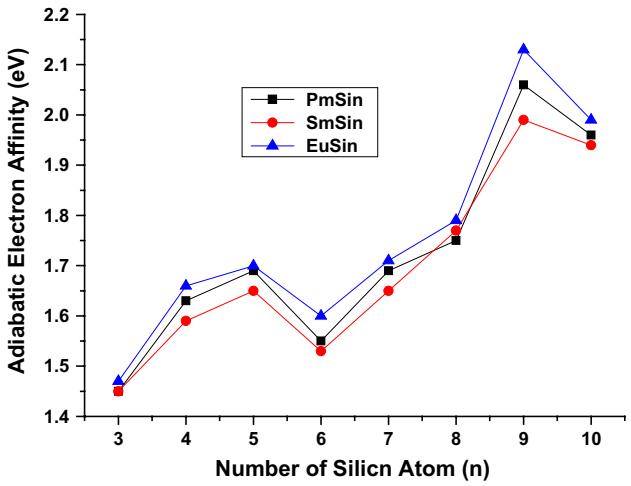

Fig. 5 Adiabatic electron affinity (AEA, in eV) $REMSi_n$ (REM = Pm, Sm, Eu, n = 3–10) calculated at the mPW2PLYP/aug-LARGE//mPW2PLYP/LARGE level of theory

HOMO–LUMO gaps of which are nearly identical. The smaller the HOMO–LUMO gap, the more easily the $PmSi_n$ tends to set off photochemical reaction. So the photochemical activity of doping Pm atom to Si clusters is very stronger than that of pure Si clusters. This property may be used to produce new functional materials such as environmental catalytic materials.

In addition, the NPA (natural population analysis) charges and valence configurations for the most stable structure are calculated at the mPW2PLYP level of theory to further understand the interaction between Pm and Si clusters. The atomic charges and configurations of Pm are listed in Table 4. Similar to other REM in small $REMSi_n$ ($n \leq 10$)

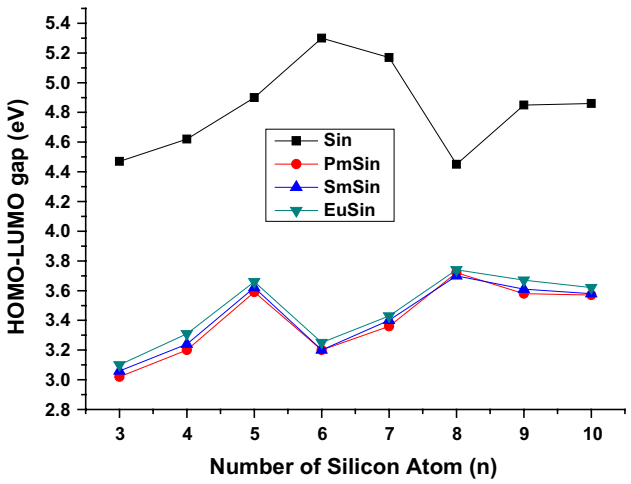

Fig. 6 HOMO-LUMO gaps (eV) of $PmSi_n$, $SmSi_n$, $EuSi_n$ and Si_n (n = 3–10) species calculated at the mPW2PLYP/aug-LARGE//mPW2PLYP/LARGE level

Table 4 Natural population analysis (NPA) valence configurations and charge of Pm atom (in a.u.) calculated with the mPW2PLYP/aug-LARGE//mPW2PLYP/LARGE scheme for the most stable structure $PmSi_n$ (n = 3 –10) clusters and their anions

Species	Electron configuration	Charge
$PmSi_3$	[core]6S(0.42)4f(4.99)5d(0.36)6p(0.09)	1.16
$PmSi_4$	[core]6S(0.24)4f(4.99)5d(0.46)6p(0.06)	1.27
$PmSi_5$	[core]6S(0.27)4f(4.99)5d(0.40)6p(0.07)	1.28
$PmSi_6$	[core]6S(0.16)4f(4.98)5d(0.52)6p(0.09)	1.24
$PmSi_7$	[core]6S(0.33)4f(4.99)5d(0.33)6p(0.09)	1.26
$PmSi_8$	[core]6S(0.15)4f(4.98)5d(0.57)6p(0.10)	1.21
$PmSi_9$	[core]6S(0.13)4f(4.97)5d(0.54)6p(0.12)	1.22
$PmSi_{10}$	[core]6S(0.36)4f(4.99)5d(0.25)6p(0.06)	1.36
$PmSi_3^-$	[core]6S(0.96)4f(4.99)5d(0.24)6p(0.32)	0.48
$PmSi_4^-$	[core]6S(0.88)4f(4.99)5d(0.24)6p(0.30)	0.58
$PmSi_5^-$	[core]6S(0.92)4f(4.99)5d(0.20)6p(0.29)	0.59
$PmSi_6^-$	[core]6S(0.87)4f(4.99)5d(0.26)6p(0.32)	0.55
$PmSi_7^-$	[core]6S(0.92)4f(4.99)5d(0.17)6p(0.27)	0.63
$PmSi_8^-$	[core]6S(0.84)4f(4.99)5d(0.27)6p(0.31)	0.60
$PmSi_9^-$	[core]6S(0.67)4f(4.99)5d(0.35)6p(0.18)	0.84
$PmSi_{10}^-$	[core]6S(0.95)4f(4.99)5d(0.11)6p(0.23)	0.71

clusters [29–33], the Pm atom in $PmSi_n$ and their anions act as an electron donor. The valence configurations of Pm are $6s^{0.13-0.42}4f^{4.97-4.99}5d^{0.25-0.57}6p^{0.06-0.12}$ and $6\ s^{0.67-0.96}4f^{4.99}5d^{0.11-0.35}6p^{0.18-0.32}$ in $PmSi_n$ (n = 3–10) and their anions, respectively. It shows that the 4*f* shell of Pm in the cluster is nearly unchanged, analogous to the situations of Sm and Eu atom in the clusters [30, 31]. The charge transfer takes place largely from 6*s* to 5*d* orbitals, leading to hybridization between 6*s* and 5*d* orbital. In the case of anion, the majority of the extra electron's charge is localized on Si_n clusters. And the mean charges of 0.63 a.u. go back to Pm from Si_n clusters (the mean charges of the anion minus the mean charges of the neutral). This weakened the bonds between Si_n clusters and Pm atom. Therefore, the DEs of Pm atom from the lowest energy structures of the anion are less than those of the neutral.

Magnetic moments are the important physical properties for compounds containing REM atoms. The magnetic moments of 6*s*, 4*f*, 5*d* and 6*p* state for Pm, total magnetic moments of Pm, and total magnetic moments of the lowest energy structures of $PmSi_n$ (n = 3–10) and their anions are shown in Table 5. The 4*f* electrons of Pm atom provide the total magnetic moments for neutral $PmSi_n$. For negatively charged ion, in addition to the 4f electrons, the 6*s* electrons of Pm also provide little magnetic moments as shown in Table 5.

4 Conclusions

The equilibrium geometries, electronic structures and electronic properties of $PmSi_n$ (n = 3–10) clusters have been systematically investigated by using the ABCluster global search technique combined with the TPSSh and mPW-2PLYP density functional methods. The results revealed that the most stable structure of neutral $PmSi_n$ and their anions belongs to substitutional structure with sextuplet and septet ground state, respectively. The reliable AEAs of $PmSi_n$ (n = 3–10) are predicted to 1.44, 1.62, 1.68, 1.55, 1.68, 1.74, 2.05 and 1.95 eV, respectively. The AEAs of $PmSi_n$ differ little from those of $SmSi_n$ and $EuSi_n$. Analyses

Table 5 Magnetic moment (μB) of 6*s*, 4*f*, 5*d* and 6*p* states for Pm atom, total magnetic moment (μB) of Pm atom, and total magnetic moment of the most stable structure of $PmSi_n$ (n = 3–10) and their anions calculated at the mPW2PLYP level

Species	Magnetic moment of Pm atom					Molecule
	6*s*	4*f*	5*d*	6*p*	Total	
$PmSi_3$	0.01	4.97	0.06	0.00	5.04	5
$PmSi_4$	0.00	4.97	0.06	0.00	5.03	5
$PmSi_5$	0.01	4.97	0.05	0.00	5.03	5
$PmSi_6$	0.01	4.96	0.06	0.01	5.04	5
$PmSi_7$	0.01	4.97	0.03	0.00	5.01	5
$PmSi_8$	0.01	4.96	0.05	0.00	5.02	5
$PmSi_9$	0.00	4.93	0.04	0.00	4.97	5
$PmSi_{10}$	0.02	4.97	0.03	0.00	5.02	5
$PmSi_3^-$	0.66	4.99	0.04	0.22	5.91	6
$PmSi_4^-$	0.66	4.88	0.10	0.25	5.89	6
$PmSi_5^-$	0.70	4.90	0.07	0.24	5.91	6
$PmSi_6^-$	0.69	4.97	0.03	0.22	5.91	6
$PmSi_7^-$	0.67	4.90	0.06	0.22	5.85	6
$PmSi_8^-$	0.68	4.97	0.02	0.21	5.88	6
$PmSi_9^-$	0.53	4.97	0.04	0.10	5.64	6
$PmSi_{10}^-$	0.71	4.94	0.03	0.20	5.88	6

of HOMO–LUMO gap showed that introducing Pm atom to Si cluster can significantly improve photochemical reactivity of the cluster. And the improved effects are as good as those of the introducing Sm and Eu atom to Si cluster. The NPA calculations indicated that the 4*f* electron of Pm atom in $PmSi_n$ (n = 3–10) and their anions hardly participates in bonding. That is, $PmSi_n$ (n = 3–10) belongs to A type. The total magnetic moments for neutral $PmSi_n$ and their anions are mainly provided by the 4*f* electrons of Pm atom. The DEs of $PmSi_n$, $SmSi_n$ and $EuSi_n$ are nearly identical. The DEs of $PmSi_n^-$, $SmSi_n^-$ and $EuSi_n^-$ are also nearly equal, and they are smaller than those of $HoSi_n^-$ and $PrSi_n^-$.

Acknowledgements This study was supported by the National Natural Science Foundation of China (Grant No. 21263010), by Program for Innovative Research Team in Universities of Inner Mongolia Autonomous Region (Gran No. NMGIRT-A1603), by the Inner Mongolia Natural Science Foundation (Grant No. 2015MS0216), and by the Inner Mongolia institutions of higher learning scientific research projects (Grant No. NJZY16419).

References

1. Ohara M, Miyajima K, Pramann A, Nakajima A, Kaya K (2002) Geometric and electronic structures of terbium–silicon mixed clusters ($TbSi_n$, $6 \le n \le 16$). J Phys Chem A 106:3702–3705
2. Koyasu K, Atobe J, Furuse S, Nakajima A (2008) Anion photoelectron spectroscopy of transition metal and lanthanide metal-silicon clusters: MSi_n^- (n = 6-20). J Chem Phys 129:214301
3. Grubisic A, Wang HP, Ko YJ, Bowen KH (2008) Photoelectron spectroscopy of europium-silicon clusters anions, $EuSi_n^-$ ($3 \le n \le 17$). J Chem Phys 129:054302
4. Grubisic A, Ko YJ, Wang HP, Bowen KH (2009) Photoelectron spectroscopy of Lanthanide-silicon cluster anions $LnSi_n^-$ ($3 \le n \le 13$, Ln = Ho, Gd, Pr, Sm, Eu, Yb): prospect for magnetic silicon-based clusters. J Am Chem Soc 131:10783–10790
5. Han JG, Hagelberg F (2009) Recent progress in the computational study of silicon and germanium clusters with transition metal impurities. J Comput Theor Nanosci 6(2):257–269
6. Zhao RN, Yuan Y, Han JG, Duan Y (2014) Actinide elements and germanium: a first-principles density functional theory investigation of the electronic and magnetic properties of ApGe (Ap = Ac–Lr) diaotms. RSC Adv 4:59331–59337
7. Hang TD, Hung HM, Nguyen MT (2016) Structural assignment, and electronic and magnetic properties of lanthanide metal doped silicon heptamers $Si_7M^{0/-}$with M = Pr, Gd and Ho†. Phys Chem Chem Phys 18:31054
8. Li XJ, Yan ZJ, Li SN (2016) The nature of structure and bonding between transition metal and mixed Si–Ge Tetramers: a 20-electron superatom system. J Comput Chem 37:2316–2323
9. Pak C, Rienstra-Kiracofe JC, Schaefer HF (2000) Electron affinities of silicon hydrides: SiH_n (n = 0–4) and Si_2H_n (n = 0–6). J Phys Chem A 104:11232–11242
10. Li XJ, Claes P, Haertelt M, Lievens P, Janssens E, Fielicke A (2016) Structural determination of niobium-doped silicon clusters by far-infrared spectroscopy and theory. Phys Chem Chem Phys 18:6291
11. Zhao RN, Han JG (2014) Geometrical stabilities and electronic properties of Si_n (n = 12–20) clusters with rare earth holmium impurity: a density functional investigation. RSC Adv 4:64410–64418
12. Beck SM (1987) Studies of silicon cluster-metal atom compound formation in a supersonic molecular beam. J Chem Phys 87(7):4233–4234
13. Koyasu K, Akutsu M, Mitsui M, Nakajima A (2005) Selective Formation of MSi_{16} (M = Sc, Ti, and V). J Am Chem Soc 127:4998–4999
14. Huang XM, Xu HG, Lu SJ, Su Y, King RB, Zhao JJ, Zheng WJ (2004) Discovery of a silicon-based ferromagnetic wheel structure in $V_xSi_{12}^-$(x = 1–3) clusters: photoelectron spectroscopy and density functional theory investigation†. Nanoscale 6:14617–14621
15. Li XJ, Han Q, Yang XH, Song RJ, Song LM (2016) Modification of alkali metals on silicon-based nanoclusters: an enhanced nonlinear optical response 659:93–99
16. Hou LY, Yang JC, Liu Yuming (2016) Reexamination of structures, stabilities, and electronic properties of holmium-doped silicon clusters $HoSi_n$ (n = 12–20). J Mol Model 22:193
17. Qi P, Jiang S (2008) Growth behavior of $La@Si_n$ (n = 1–21) metal-encapsulated clusters. J Chem Phys 128:084711
18. Cao TT, Feng XJ, Zhao LX, Liang X, Lei YM, Luo YH (2008) Structure and magnetic properties of La-doped Si_n (n = 1–12,24) clusters: a density functional theory investigation. Eur Phys J D 49:343–351
19. Feng YT, Yang JC (2017) Stability and electronic properties of praseodymium-doped silicon clusters PrSin (n = 12–21). J Mol Model 23:180
20. Li CG, Pan LJ, Shao P, Ding LP, Feng HT, Luo DB, Liu B (2015) Structures, stabilities, and electronic properties of the neutral and anionic Si_nSm^{λ} (n = 1–9, λ = 0, − 1) clusters: comparison with pure silicon clusters. Theor Chem Acc 134:34
21. Zhao GF, Sun JM, Gu YZ, Wang YX (2009) Density-functional study of structural, electronic, and magnetic properties of the $EuSi_n$ (n = 1–13) clusters. J Chem Phys 131:114312
22. Wang J, Liu Y, Li YC (2010) Magnetic silicon fullerene. Phys Chem Chem Phys 12:11428–11431
23. Liu TG, Zhao GF, Wang YX (2011) Structural, electronic and magnetic properties of $GdSi_n$ (n = 1–17) clusters: a density functional study. Phys Lett A 375:1120–1127
24. Liu TG, Zhang WQ, Li YL (2014) First-principles study on the structure, electronic and magnetic properties of $HoSi_n$ (n = 1–12, 20) clusters. Front Phys 9:210–218
25. Zhao RN, Ren ZY, Guo P, Bai JT, Zhang CH, Han JG (2006) Geometries and electronic properties of the neutral and charged rare earth Yb-doped Si_n(n = 1–6) clusters: a relativistic density functional investigation. J Phys Chem A 110:4071–4079
26. Zhao RN, Han JG, Bai JT, Liu FY, Sheng LS (2010) The medium-sized charged $YbSi_n^{\pm}$ (n = 7–13) clusters: a relativistic computational investigation. Chem Phys 378:82–87
27. Zhao RN, Han JG, Bai JT, Liu FY, Sheng LS (2010) A relativistic density functional study of Si_n (n = 7–13) clusters with rare earth ytterbium impurity. Chem Phys 372:89–95
28. Cao TT, Zhao LX, Feng XJ, Lei YM, Luo YH (2009) Structural and electronic properties of $LuSi_n$ (n = 1–12) clusters: a density functional theory investigation. J Mol Struct THEOCHEM 895:148–155
29. Feng YT, Yang JC, Liu YM (2016) Study on the structures and properties of praseodymium-doped silicon clusters PrSin (n = 3–9) and their anions with density functional schemes. Theor Chem Acc 135:258
30. Xie XH, Hao DS, Liu YM, Yang JC (2015) Samarium doped silicon clusters $SmSi_n$ (n = 3–10) and their anions: structures, thermochemistry, electron affinities, and magnetic moments. Comput Theor Chem 1074:1–8
31. Yang JC, Wang J, Hao YR (2015) Europium-doped silicon clusters $EuSi_n$ (n = 3–11) and their anions: structures, thermochemistry, electron affinities, and magnetic moments. Theor Chem Acc 134:81

32. Yang JC, Feng YT, Xie XH, Wu HW, Liu YM (2016) Gadolinium-doped silicon clusters GdSin (n = 2–9) and their anions: structures, thermochemistry, electron affinities, and magnetic moments. Theor Chem Acc 135:204
33. Hou LY, Yang JC, Liu YM (2017) Density-functional study of the structures and properties of holmium-doped silicon clusters HoSin (n = 3–9) and their anions. J Mol Model 23:117
34. Xie XH, Hao DS, Yang JC (2015) Ytterbium doped silicon clusters $YbSi_n$ (n = 4-10) and their anions: structures, thermochemistry, and electron affinities. Chem Phys 461:11–19
35. He S, Yang JC (2017) Study on structure and property of lutetium introduced silicon clusters $LuSi_n$ (n = 3–10) and their anions with density functional theory. J Clust Sci. doi:10.1007/s10876-017-1225-x
36. Schwabe T, Grimme S (2006) Towards chemical accuracy for the thermodynamics of large molecules: new hybrid density functionals including non-local correlation effects. Phys Chem Chem Phys 8:4398–4401
37. Zhang J, Dolg M (2015) ABCluster: the artificial bee colony algorithm for cluster global optimization. Phys Chem Chem Phys 17:24173–24181
38. Frisch MJ, Trucks GW, Schlegel HB, Scuseria GE, Robb MA, Cheeseman JR, Scalmani G, Barone V, Mennucci B, Petersson GA, Nakatsuji H, Caricato M, Li X, Hratchian HP, Izmaylov AF, Bloino J, Zheng G, Sonnenberg JL, Hada M, Ehara M, Toyota K, Fukuda R, Hasegawa J, Ishida M, Nakajima T, Honda Y, Kitao O, Nakai H, Vreven T, JA Montgomery Jr, Peralta JE, Ogliaro F, Bearpark M, Heyd JJ, Brothers E, Kudin KN, Staroverov VN, Keith T, Kobayashi R, Normand J, Raghavachari K, Rendell A, Burant JC, Iyengar SS, Tomasi J, Cossi M, Rega N, Millam JM, Klene M, Knox JE, Cross JB, Bakken V, Adamo C, Jaramillo J, Gomperts R, Stratmann RE, Yazyev O, Austin AJ, Cammi R, Pomelli C, Ochterski JW, Martin RL, Morokuma K, Zakrzewski VG, Voth GA, Salvador P, Dannenberg JJ, Dapprich S, Daniels AD, Farkas Ö, Foresman JB, Ortiz JV, Cioslowski J, Fox DJ (2010) Gaussian 09 revision C.01. Gaussian Inc, Wallingford
39. Staroverov VN, Scuseria GE, Tao J (2003) Comparative assessment of a new nonempirical density functional: molecules and hydrogen-bonded complexes. J Chem Phys 119:12129–12137
40. Dolg M, Stoll H, Savin A, Preuss H (1989) Energy-adjusted pseudopotentials for the rare earth elements. Theor Chim Acta 75:173–194
41. Feller D (1996) The role of databases in support of computational chemistry calculations. J Comput Chem 17:1571–1586
42. Schuchardt KL, Didier BT, Elsethagen T (2007) Basis set exchange: a community database for computational sciences. J Chem Inf Model 47(3):1045–1052
43. Woon DE, Dunning TH (1993) Gaussian basis sets for use in correlated molecular calculations. II. The atoms aluminum through argon. J Chem Phys 98:1358–1371
44. Buchachenko AA, Chalasiński G, Szeześniak MM (2007) Diffuse basis functions for small-core relativistic pseudopotential basis sets and static dipole polarizabilities of selected lanthanides La, Sm, Eu, Tm and Yb. Struct Chem 18:769–772
45. Cao X, Dolg M (2002) Segmented contraction scheme for small-core lanthanide pseudopotential basis sets. J Mol Struct THEOCHEM 581:139–147
46. Raghavachari K (1986) Theoretical study of small silicon clusters: equilibrium geometries and electronic structures of Sin (n = 2–7,10). J Chem Phys 184:5672–5686
47. Yang JC, Xu WG, Xiao WS (2005) The small silicon clusters Si_n, (n = 2–10) and their anions: structures, themochemistry, and electron affinities. J Mol Struct (THEOCHEM) 719:89–102
48. Zhu X, Zeng XC (2003) Structures and stabilities of small silicon clusters: Ab initio molecular-orbital calculations of Si_7–Si_{11}. J Chem Phys 118:3558–3570